International Journal of Pharmaceutical and Bio-Medical Science

ISSN(print): 2767-827X, ISSN(online): 2767-830X

Volume 04 Issue 12 December 2024

Page No : 954-968

DOI: https://doi.org/10.47191/ijpbms/v4-i12-07,Impact Factor:7.792

Investigation of ROS-Driven Cytotoxic Mechanisms in WO_3: Ag Heterostructures Supported on Carbon against Bladder Cancer

Bruna D. L. Fragelli[1], Joice M. A. Rodolpho[2], Krissia F. Godoy[2], Laura O. Líbero[1], Luis I. Granone[4], Maria S. Churio[4], Ana. C. M. Rennó[3], Fernanda F. Anibal[2], Elson Longo[1], Marcelo Assis[3]

[1] Center for Development of Functional Materials, Federal University of São Carlos (UFSCar), 13565-905, São Carlos, SP, Brazil.

[2] Laboratory of Inflammation and Infectious Diseases, Department of Morphology and Pathology, Federal University of São Carlos (UFSCar), 13565-905, São Carlos, SP, Brazil.

[3] Department of Biosciences, Federal University of São Paulo (UNIFESP), 11015-020, Santos, SP, Brazil.

[4]Chemistry Departament, (IFIMAR), CONICET, Universidad Nacional de Mar del Plata (UNMdP), B7602, Mar del Plata, Argentina.

Bruna D. L. Fragelli: 0000-0002-3970-7834
Joice M. A. Rodolpho: 0000-0002-1277-0083
Krissia F. Godoy: 0000-0002-0493-2329
Laura O. Líbero: 0000-0003-0286-6257
Luis I. Granone: 0000-0002-8733-2942
Maria S, Churio: 0000-0003-1239-6367
Ana C. M. Rennó: 0000-0002-8906-5390
Fernanda F. Anibal: 0000-0003-0571-8516
Elson Longo: 0000-0001-8062-7791
Marcelo Assis: 0000-0003-0355-5565

ABSTRACT

Bladder cancer presents a significant health challenge due to its high malignancy and rising incidence rates. Silver-based materials are well-known for their cytotoxic effects on various cell types. This study not only aimed to synthesize and characterize carbon-supported WO_3:Ag heterostructures but also to evaluate their biological and physicochemical properties. The material was synthesized through the synergistic thermal decomposition of α-Ag_2WO_4 dispersed in chitosan, followed by WO_3:Ag heterostructure formation on a carbon support, yielding samples with varying α-Ag_2WO_4 concentrations (SC, SC1, SC2, and SC4, for 0, 10, 20 and 40% of α-Ag_2WO_4 for chitosan). Characterization confirmed the successful formation of carbon-supported heterostructures with controlled ionic release and enhanced ROS generation. *In vitro* assays were conducted to assess the viability of non-tumor (3T3 fibroblasts) and tumor (bladder carcinoma MB49) cells using MTT salt and neutral red dye. Additional analyses included autophagy detection by correlating data from viability assays, nitric oxide and ROS quantification using the Griess reaction and fluorescent probes, and Caspase-3 activity measured with a fluorescent antibody. The results indicated that SC1 and SC2 samples were more effective against both cell types, with SC2 showing heightened effectiveness against the tumor lineage by inducing greater oxidative stress in MB49 cells compared to 3T3 fibroblasts. Additionally, the materials exhibited low ionic release (<0.01%), reducing potential adverse effects. Mechanistic analysis showed that the carbon support and synergistic interactions between WO_3 and Ag modulated •OH radical production, even without light, enhancing the material's cytotoxic efficiency. These findings highlight the therapeutic potential of WO_3:Ag heterostructures as a safe and effective approach for treating aggressive cancers like bladder carcinoma, emphasizing the importance of further development in advanced biofunctional materials. This study also highlights the therapeutic

ARTICLE DETAILS

Published On:
14 December 2024

potential of carbon-supported WO_3:Ag heterostructures in bladder cancer treatment and underscores the importance of continued research in the development of novel anticancer strategies.

KEYWORD: heterostructures; carbon support; blader cancer; oxidative stress;apoptosis.

Available on:
https://ijpbms.com/

1. INTRODUCTION

In Western countries, bladder cancer (BC) is among the leading causes of cancer-related deaths, ranking as the ninth most common cancer globally [1]. In 2020, there were approximately 573,000 new cases and 213,000 deaths, with a global five-year prevalence of 1,721,000 cases [2]. BC is a significant health issue, with its overall incidence remaining stable; however, certain regions have experienced increased morbidity and mortality, likely due to varying exposure factors linked to cancer development [3]. Although progress in clinical management over the past three decades has been modest, recent advancements have shifted this trend. The identification of various DNA, RNA, and protein biomarkers through sequencing and gene expression has deepened our understanding of BC, revealing it to be one of the malignancies with the highest mutation rates, second only to lung and skin cancers [4]. A particularly aggressive and challenging subtype of BC is represented by the MB49 murine cell line, which is commonly used as a model for studying bladder cancer [5–8]. MB49 cells exhibit high malignancy and resistance to conventional therapies, making them a valuable tool for researching new treatment strategies [9]. This highlights the urgent need for innovative treatments that are easily synthesized, safe, and adaptable, particularly given the significant heterogeneity among different types of bladder cancer. Such treatments must offer greater selectivity and lower risks of side effects [10].

The emerging field of advanced materials is focused on developing personalized multifunctional particles with diverse applications in healthcare, including cancer therapy [11]. Ag-based materials are particularly notable for their physicochemical, antimicrobial, and anti-inflammatory properties, making them promising candidates for biomedical applications [12,13]. Additionally, Ag is less toxic than metals like mercury and copper, which enhances its appeal for medical use [14,15]. However, their clinical use remains limited. Consequently, the development of advanced materials that incorporate Ag along with other components is being investigated, as these formulations may enhance biofunctionality and reduce cytotoxicity in eukaryotic cells [16–20]. In this context, understanding the toxicity and environmental impact of these new materials is crucial, particularly for their application as potential anticancer agents. By addressing these factors, we can facilitate the development of safe and effective treatments that also consider environmental sustainability.

One promising Ag-based material is silver semiconductors, particularly α-Ag_2WO_4, which has become the focus of our research group due to its antimicrobial, catalytic, and antitumor properties [21]. Previous studies have demonstrated the effectiveness of these materials in combating various pathogenic microorganisms, including resistant bacteria, fungi, and viruses [22–27]. Furthermore, this material has proven efficient as a catalyst for the remediation of organic pollutants and the oxidation of sulfides [28,29]. Recently, studies on the toxicity of this material have also been increasing, aiming to address gaps in biosafety and the environmental impact of such materials [30–32] . The anticancer potential of α-Ag_2WO_4 has also been evaluated against bladder cancer using the MB49 cell line[33] . It was observed that when modified by electron or laser irradiation, which generates silver nanoparticles on the surface of α-Ag_2WO_4, the material exhibits enhanced efficacy in eliminating these cells. However, obtaining Ag nanoparticles on the surface of α-Ag_2WO_4 through these methods remains challenging. An alternative approach for creating these heterostructures may involve the thermal degradation of α-Ag_2WO_4, transforming it into WO_3:Ag. This strategy could be advantageous for modulating the properties of this class of materials.

Understanding the interaction between the α-Ag_2WO_4 and cells is crucial. One aspect is the ability of a material to be internalized by the cell, which is fundamental for its bioactivity, especially in the case of metal-based nanoparticles, which have distinct characteristics in this context [34]. Electrostatic interaction plays an important role in initial adhesion and cellular recognition, directly influencing how materials are biologically perceived [35]. Additionally, these nanoparticles also have the ability to release compositional ions (Ag^+ and W^{6+}) into the cellular environment, triggering a series of intracellular processes. The generation of reactive oxygen species (ROS) by these particles can also have significant consequences on cellular components, resulting in a variety of effects, from modifications in normal cellular processes to more severe damage [36–38] . The complexity of this interaction between materials and cells underscores the urgency to explore and understand the biological implications of these materials at a deeper level.

In this study, WO_3:Ag heterostructures supported on carbon were synthesized to evaluate their cytotoxicity on healthy murine fibroblast NIH/3T3 cells and bladder cancer MB49 cells. The carbon support was utilized to modulate

ROS production by the heterostructure and enhance stability, thereby reducing unwanted effects from ionic release of Ag^{+} and W^{6+}. These materials were characterized using thermogravimetric analysis (TG/DTA), X-ray diffraction (XRD), Raman spectroscopy, scanning electron microscopy (SEM), and energy-dispersive X-ray spectroscopy (EDS). Cytotoxic activity was assessed using the MTT assay and neutral red dye on both bladder cancer and murine fibroblast cell lines. Intracellular production of RNS and ROS was analyzed using the Griess reaction and the 2',7'-dichlorodihydrofluorescein diacetate probe, respectively. Cellular morphology was examined via optical microscopy, and caspase-3 levels were evaluated. The mechanism of action of the samples was assessed directly through the production of •OH radicals using EPR, and indirectly by measuring the reduction in photocatalytic efficiency during RhB discoloration using specific reactive scavengers. Ionic release was evaluated using ICP-OES. Finally, we propose a radical formation mechanism, linking the release of ROS to the cytotoxic effects observed in the cell lines. This work aims to provide insights for the development of new biofunctional materials, particularly for the treatment of bladder cancer, which is extremely aggressive and challenging to treat.

2. MATERIAL AND METHODS

2.1 Synthesis

Synthesis of α-Ag_2WO_4: The synthesis of α-Ag_2WO_4 was carried out following the procedure described in previous studies [39,40]. The coprecipitation method in an aqueous medium was employed. In two separate beakers, 50.0 mL of distilled water was added, and $1x10^{-3}$ mol of $Na_2WO_4.2H_2O$ (99.9%, Sigma-Aldrich) and $2x10^{-3}$ mol of $AgNO_3$ (Cennabras, 99.8%), respectively, were dissolved in the solutions. Once the compounds were completely dissolved, the solutions were heated to 70°C, and the $AgNO_3$ solution was added to the $Na_2WO_4.2H_2O$ solution, resulting in the formation of a white precipitate. The solution was stirred continuously for 20 minutes and then centrifuged. The precipitate was washed with distilled water until the pH 7. Finally, the precipitate was dried at 60°C for 12 hours.

Synthesis of WO_3:Ag Supported on Carbon: In a beaker, 0.100 g of chitosan (medium molecular weight, Sigma-Aldrich) was added to 20.0 mL of ethanol and dispersed using ultrasound for 5 minutes. In another beaker, separate dispersions of 0.01 g, 0.02 g, and 0.04 g of α-Ag_2WO_4 were prepared by adding each respective amount to 20.0 mL of ethanol and dispersing for 5 minutes. After this step, the α-Ag_2WO_4 dispersion was added to the chitosan dispersion and mixed for 10 minutes. The resulting mixture was then dried in an oven at 60 °C for 5 hours. After drying, the material was further heated in a conventional oven at 400 °C for 30 minutes, resulting in the final material. The samples without α-Ag_2WO_4 and with 10%, 20%, and 40% (w/w) of α-Ag_2WO_4 were labeled as SC, SC1, SC2, and SC4, respectively.

2.2 Characterization

The thermal stability analysis of the samples was conducted using a thermogravimetric analyzer/differential thermal analyzer (TG/DTA) NETZSCH—409 Cell. The analysis was performed in an oxygen atmosphere with a flow rate of 50 Ml/min, and the temperature range was set from 25 to 1000 °C with a heating rate of 10 °C/min. X-ray diffraction (XRD) analyses were carried out using a Rigaku diffractometer equipped with Cu Kα radiation (λ = 1.5406 Å). The measurements were obtained with a step size of 0.02° in the angular range of 10° to 110°. Raman spectra were collected using an Ihr550 spectrometer (Horiba Jobin Yvon) coupled with an Ag ion laser (MellesGriot) operating at a wavelength of 633 nm. The laser had a maximum power of 200 Mw, and a fiber microscope was used for data collection. The spectra were recorded in the range of 100-3000 cm^{-1}. The morphology and composition of the samples were analyzed using a scanning electron microscope LEO 440i (Leica-Zeiss) coupled with an X-ray dispersive energy spectroscopy (EDX) detector Oxford – INCA 250. Images of the samples were obtained, and the elemental composition was determined using EDX. The ionic release tests were carried out following the same procedure as the *in vitro* assays. The materials were incubated for 24 hours at 37°C in the previously determined concentrations. After incubation, the solution was acidified using a 1M HNO_3 solution and subjected to analysis using an ICP-OES (inductively coupled plasma optical emission spectrometry) instrument, specifically an ICP-OES Icap 7000.

2.3 ROS identification

Scavenger tests: For the analysis of the reactive species produced by the samples, photodegradation tests of rhodamine B (RhB, Synth) were conducted. Specific scavengers were added to determine the contribution of different reactive species, including hydroxyl radical (•OH, potassium acid phthalate, $C_8H_5KO_4$, Aldrich), hydroperoxyl radical (•OOH, p-benzoquinone, $C_6H_4O_2$, Alfa-Aesar), singlete oxygen ($^1O_2$, ascorbic acid, C6H8O6, Synth), holes (h^+, ammonium oxalate, $(NH_4)_2C_2O_4$, Aldrich), and electrons (e^-, copper nitrate, $Cu(NO_3)_2•3H_2O$, Aldrich). The procedure involved adding 50 mg of the sample and $1×10^{-5}$ mol of the specific scavenger to a 50 mL solution of RhB ($1×10^{-5}$ M). A blank system without the scavenger was also prepared. The systems were then sonicated for 5 minutes and transferred to a glass reactor equipped with a water circulator to maintain a temperature of 25°C. To allow for adsorptive processes, the systems were kept in the dark under stirring for 30 minutes. Subsequently, visible lamps (6 visible lamps, 15W, Philips TL-D) were turned on, and the samples were exposed to light for 2 hours. At specific time intervals, aliquots were taken and analyzed using a spectrophotometer to monitor the absorption band of RhB at 556 nm. The inhibition of photodegradation with the addition of scavengers was used to determine the production of reactive species. The results were always

normalized by comparing them to the test without the addition of scavenger, allowing for a proportional assessment of reactive species production.

Hydroxyl radical detection: For the detection of hydroxyl radicals (•OH), a solution of 5,5-dimethyl-1-pyrroline N-oxide (DMPO, 99%, Sigma-Aldrich) was prepared. Specifically, 10 µL of the DMPO solution was placed in contact with the material in the absence of light. An aliquot of this mixture was then transferred to a cylindrical quartz tube for examination using Electron Paramagnetic Resonance (EPR). The EPR instrument was set to the following parameters: a frequency of 9.59816 GHz, a modulation frequency of 100 kHz, a central field of 3420 G, a sweep width of 200 G, a modulation amplitude of 2 G, a conversion time of 40 ms, a sweep time of 41 s, an attenuation of 10 dB, and a power of 20.37 mW. The EPR spectrum was obtained by averaging 20 scans.

2.4 *In vitro* assays

The murine fibroblast cell line NIH/3T3 was used[41] and non-invasive bladder carcinoma cell lines from male C57BL/6 mouse [42]. The tested concentrations of the samples were: 3.9, 7.8, 15.62, 31.25, and 62.5 µg/mL. Tests were performed at least in octuplicate (N= 8), as part of three independent experiments. The tests conducted included the evaluation of cell viability through analysis of mitochondrial function and membrane integrity [43,44], activation of the cell death process through autophagy by arbitrary autophagic units (AAU) [45], measurement of reactive nitrogen species (RNS), such as Nitric Oxide (NO), using the Griess Reaction [46–48], detection of reactive oxygen species (ROS), quantification of Caspase-3 levels, and examination of cell morphology through optical microscopy. Detailed experimental procedures for these techniques can be found in the Supplementary Information.

3. RESULTS

3.1 Characterization

The first process investigated was the thermal decomposition of the final material using TG/DTA analysis (**Figure 1A**). The results showed that α-Ag_2WO_4 alone begins to degrade at approximately 550 °C, while chitosan experiences significant mass loss related to its carbonization process starting at 220 °C. For samples SC1, SC2, and SC4, mass loss was observed starting from 220 °C, with degradation beginning at 200 °C. This indicates an associative process between the combustion of the organic matter from chitosan and the thermal degradation of α-Ag_2WO_4. The thermal decomposition of α-Ag_2WO_4 leads to the formation of WO_3:Ag heterostructures. Due to the carbonization of chitosan, the degradation of α-Ag_2WO_4 occurred at lower temperatures than expected. The carbon combustion facilitated the formation of WO_3:Ag at 400 °C, a temperature selected to ensure complete carbonization of the chitosan. This thermal treatment approach was specifically designed to improve the stability of the WO_3 heterostructure and control its cytotoxic effects. By immobilizing the heterostructure in a carbon matrix, it is expected that the release of Ag^+ and W^{6+} ions, along with the production of reactive oxygen species (ROS), will be more controlled compared to α-Ag_2WO_4, enhancing its viability as a potential therapeutic agent.

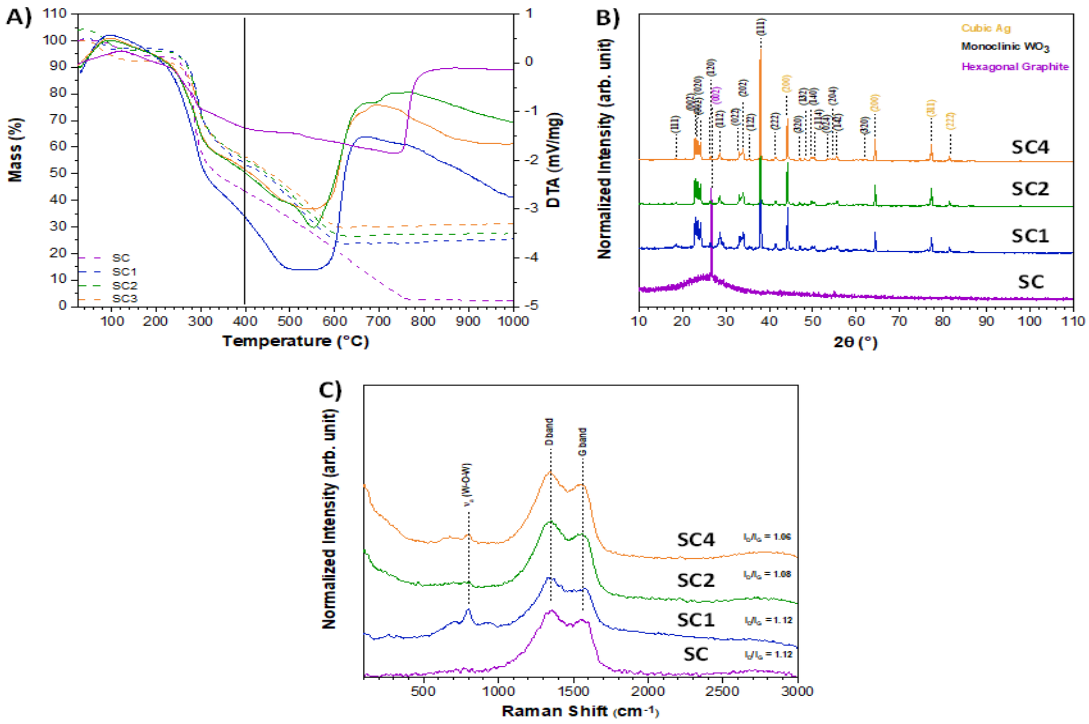

Figure 1. A) TG/DTA, B) XRD patterns and C) Raman spectra of the samples.

To analyze the structural properties of the samples after thermal treatment, XRD analyses were conducted (**Figure 1B**). It can be observed that the QT sample completely transforms into graphite with a hexagonal structure and *P63mc* space group [49] . As for the SC1, SC2, and SC4 samples, in addition to the formation of graphite, the complete decomposition of α-Ag_2WO_4 into WO_3 (monoclinic with space group *P21/c*) and Ag (cubic with space group *Fm-3m*) is observed [50,51]. This indicates that the atmosphere generated during the combustion of chitosan promotes redox processes for the formation of WO_3 and Ag. To complement the XRD analysis, Raman spectroscopy analyses were performed, as shown in **Figure 1C**. It is possible to observe the D (~1350 cm^{-1}) and G (~1570 cm^{-1}) bands of carbon-based materials, which correspond to defects in the graphite layers and sp^2 hybridized carbon bonds, respectively [52]. The intensity ratio between these two bands (ID/IG) is directly related to the degree of defects in the material [53]. The obtained I_D/I_G values slightly decrease with increasing WO_3:Ag loading, ranging from 1.12 to 1.06. This indicates a reduction in the defects present in the carbon support material with the increase in WO_3:Ag load. Additionally, a peak at 799 cm^{-1} can be observed, corresponding to the stretching mode of W-O-W bonds. These findings are consistent with the results obtained from Raman spectroscopy and XRD analysis.

SEM images are presented in **Figure 2**. It can be observed that carbon support material exhibits an extremely porous micrometric structure (**Figure 2A**). Upon the formation of WO3/Ag on the surface of the carbonic material, irregular structures of these materials (highlighted as high-contrast particles) fill these pores and deposit on the surface of the carbonic support (**Figure 2B-C**). As anticipated, with increasing concentrations of WO_3:Ag, the surface becomes progressively filled with these structures. **Figure S1** displays the elemental mapping of Ag, W, and O species, revealing a non-uniform distribution of these particles on the carbon support surface.

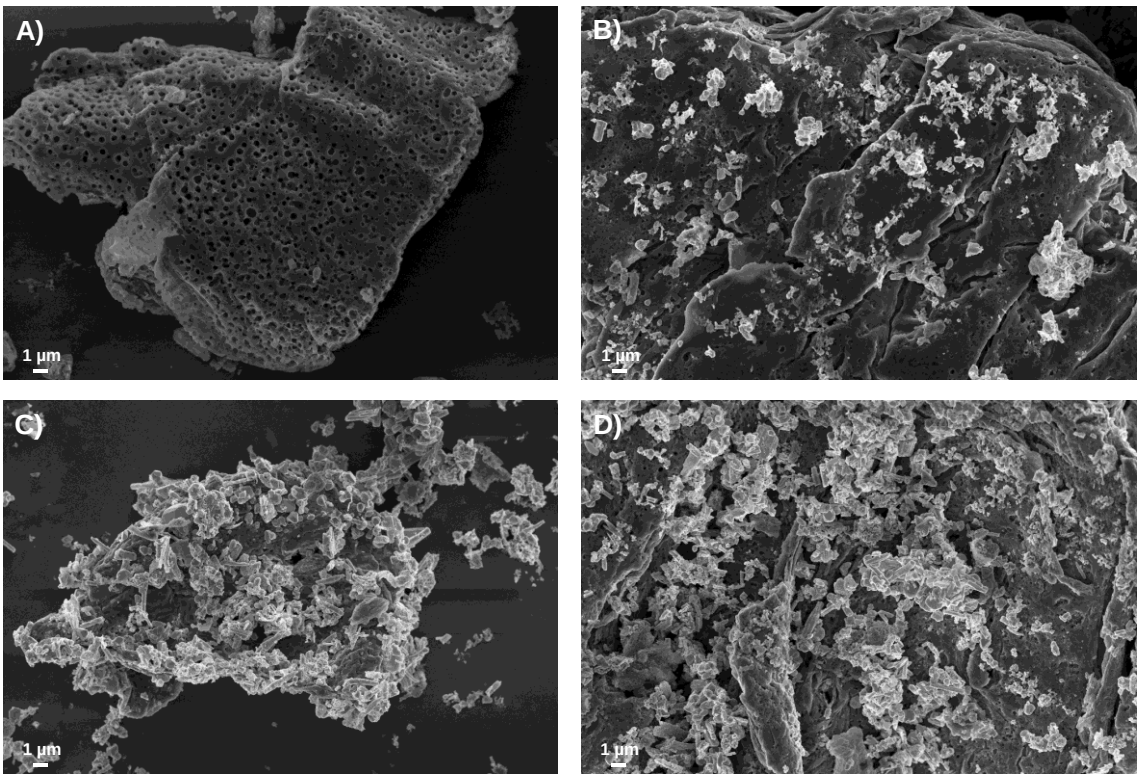

Figure 2. SEM images of the samples A) SC; B) SC1; C) SC2 and; D) SC4.

3.2 Cellular Assays

The 3T3 mouse fibroblast cells are widely used in cytotoxicity assays due to their sensitivity to various toxic substances such as nanomaterials [54,55]. On the other hand, the MB49 cell line, derived from mouse bladder carcinoma, is notably more resistant, especially to conventional treatments, making it more challenging in terms of cytotoxicity induction[56].

Figure **3** shows the results obtained by the MTT method in this study, where the 3T3 cells demonstrated a significant decrease in cell viability at the highest concentrations tested of the samples SC1, SC2, and SC4 when compared to the control. **Figures 3B** and **3D** show a reduction starting at the concentration of 7.8 µg/mL, and **Figure 3C** shows a reduction starting at 15.62 µg/mL. The same pattern was observed in the results obtained by the VN technique, which also demonstrated a reduction in viability in the SC1, SC2, and SC4 samples. **Figures 3F** and **3H** show a significant decrease starting at the concentration of 3.9

µg/mL, and **Figure 3G** shows a reduction starting at 15.62 µg/mL.

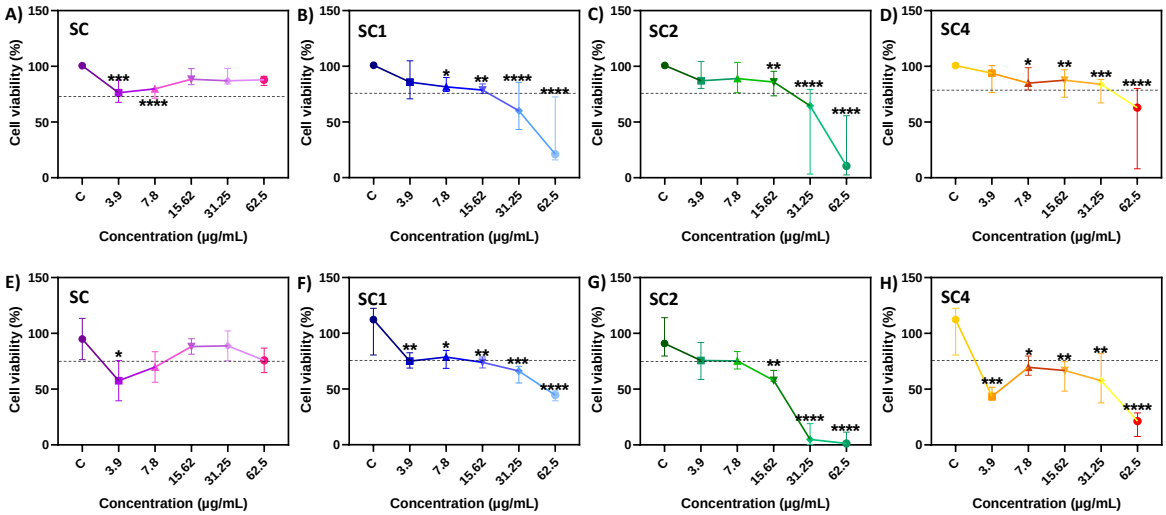

Figure 3. *In vitro* results in murine fibroblast NIH/3T3 cell line. A-D) Cell viability in % with MTT. E-H) Cell viability in % with Neutral Red. (*) vs C: *p ≤0.05; **p ≤0.01; ***p ≤0.001; ****p ≤0.0001. The results were presented as median with upper and lower quartiles: Me [Q1; Q3].

Figure 4 shows the cell viability results by MTT and VN in the MB49 cell model, highlighting a reduction in cell viability by the MTT assay at a concentration of 62.5 µg/mL compared to the control in samples SC1, SC2, and SC4 (**Figures 4B**, **4C**, and **4D**, respectively). For the VN assay, the results showed that the decrease in MB49 viability was significant for sample SC1 at a concentration of 62.5 µg/mL (**Figure 4F**), and for sample SC2 it was from a concentration of 7.8 µg/mL (**Figure 4G**).

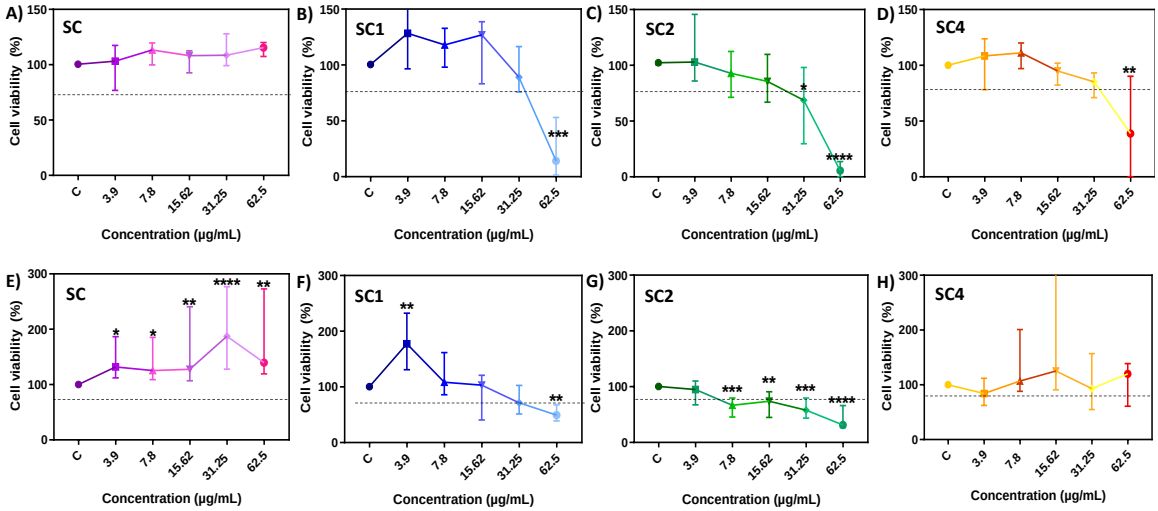

Figure 4. *In vitro* results in murine bladder cancer cell line MB49. A-D) Cell viability in % with MTT. E-H) Cell viability in % with Neutral Red. (*) vs C: *p ≤0.05; **p ≤0.01; ***p ≤0.001; ****p ≤0.0001. The results were presented as median with upper and lower quartiles: Me [Q1; Q3].

These results showed that, although the SC1 and SC2 samples exhibited lower cytotoxic potential for MB49 cells compared to 3T3 cells, there was still a significant reduction in the viability of MB49 cancer cells at the higher concentrations of SC1 and SC2 compared to the control group. These data are corroborated by optical microscopy images that can be found in the Supplementary Information (Figures S2-S9) These data are considered promising as they suggest that these materials have potential to be explored as an anticancer treatment, given that they affected the viability of malignant cells. Studies in the literature have shown that compounds previously tested in the MB49 cell line, when

compared to fibroblast cells, produced results similar to those identified in this study [57].

Both cell viability and mitochondrial membrane integrity can be affected by several factors, including redox transitions, which can lead to consequences such as ischemia/reperfusion through contact with nanoparticles [58]. These redox transitions are analyzed through the production of reactive oxygen species (ROS) in MB49 cells, as described in **Figure 5**.

The results in **Figure 5B** showed that, although not statistically significant, the SC1 and SC2 groups tend to increase ROS production gradually with the increase in the tested concentration. The production of ROS at high concentrations causes intracellular oxidative stress, which can lead to cellular damage, inducing programmed cell death through signaling proteins such as caspase-3 [59,60].

Caspase-3, also known as the effector caspase, is a protein responsible for the final degradation of substrates that activate the caspase-dependent apoptotic pathway [61]. The analyses for caspase-3 in this study demonstrated in MB49 cells that, although not statistically significant, there was an increase in caspase production at a concentration of 3.9 µg/mL compared to the control (**Figure 5C**). Cell death by autophagy induced by SC, SC1, SC2, and SC4 is shown in the Supplementary Information (Figures S10 and S11). Cell death by autophagy occurred in all materials.

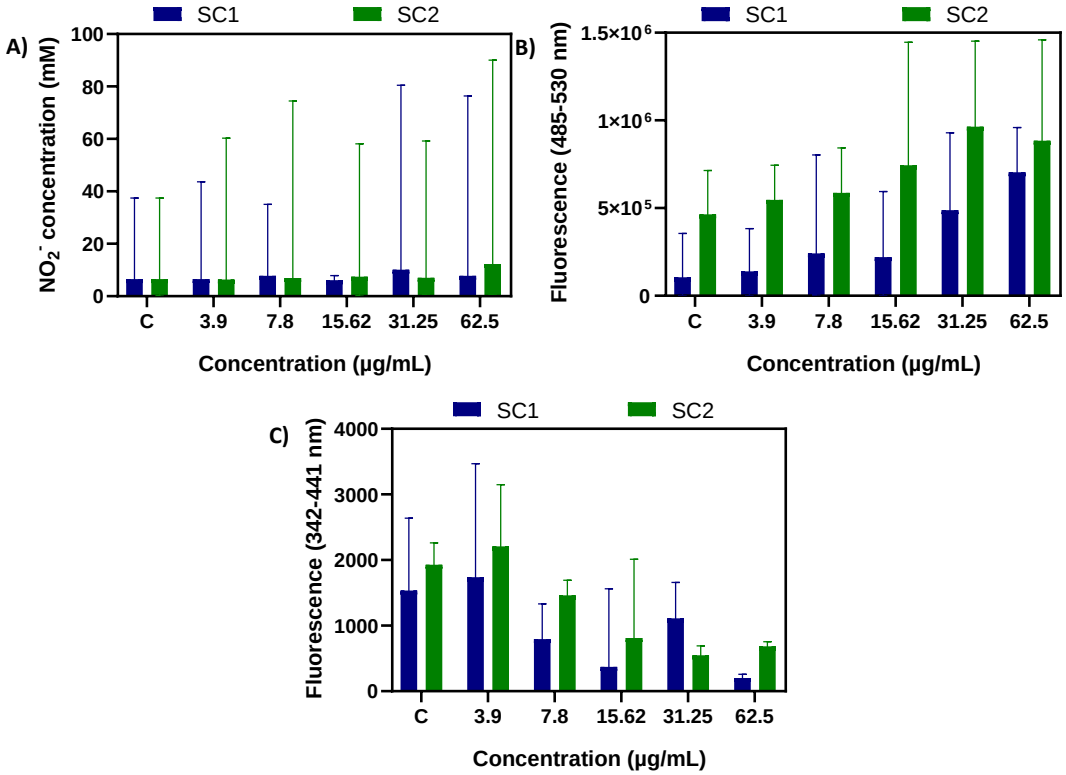

Figure 5. ***In vitro*** **results of SC1 vs SC2 in murine bladder cancer cell line MB49. A) NO intracellular synthesis. B) ROS intracellular synthesis. C) Caspase-3 levels. (*) vs SC1: *p ≤0.05; **p ≤0.01. The results were presented as median with upper and lower quartiles: Me [Q1; Q3].**

It is believed that the exposure of nanomaterials in MB49 cells may interfere with cell-to-cell interaction by triggering the activation of the intrinsic apoptosis pathway, as observed through caspase-3 [62]. When there is an increase in ROS production and consequently activation of the caspase-3 pathway, cells enter a state of vulnerability, facilitating the initiation of the apoptotic process [63,64]. These factors are crucial to evaluate in maintaining cellular integrity and functionality.

3.3 Mechanistic Insights

The cellular activity of the samples can be attributed to various mechanisms associated with the samples, such as ionic release, generation of reactive oxygen species (ROS), and physical contact [65,66]. In order to investigate these effects, the ROS production of the material was assessed using electron paramagnetic resonance (EPR) (**Figure 6A**), while the photoreactive scavengers were employed to examine their impact (**Figure 6B**). Furthermore, the ionic release was analyzed through inductively coupled plasma optical emission spectrometry (ICP-OES) (**Figure 6C**) to shed light on this aspect.

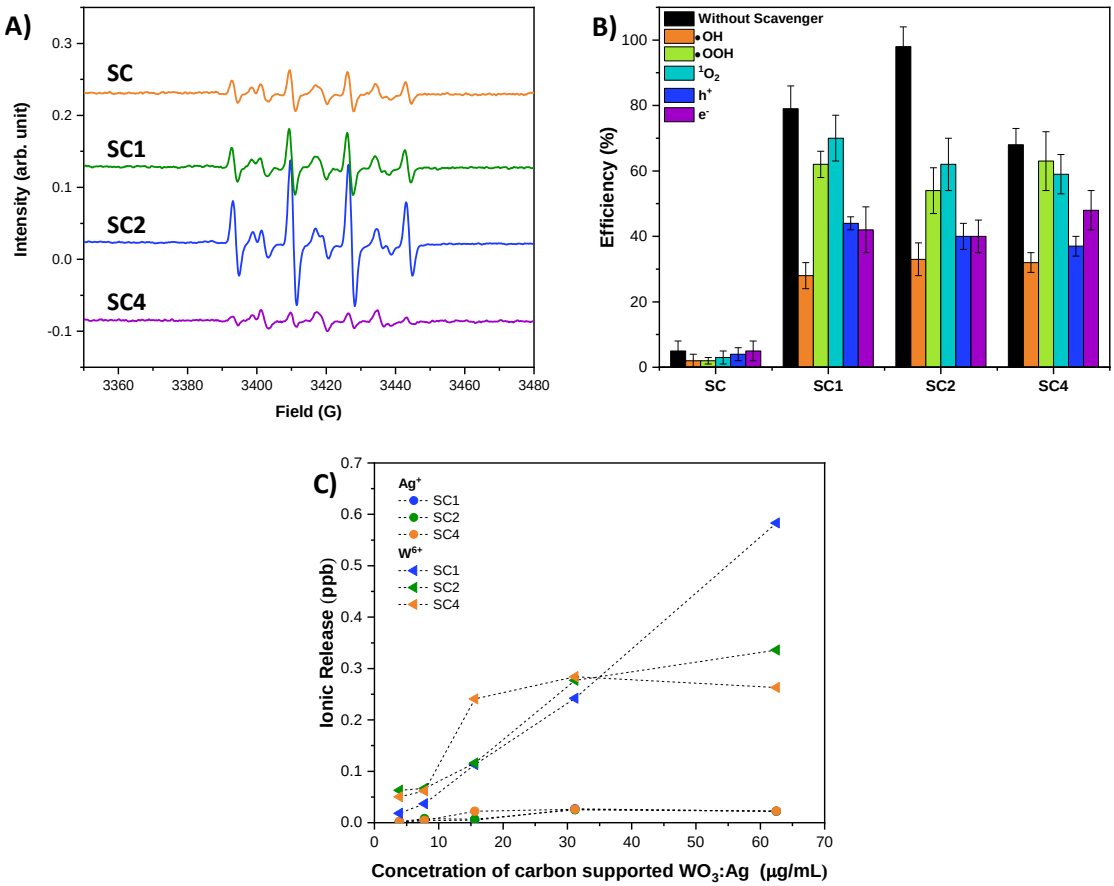

Figure 6. A) Detection of •OH using DMPO by EPR; B) Efficiency in the photodegradation of RhB by the addition of scavengers of reactive species; C) Ionic release of Ag^+ and W^{6+} in samples at different concentrations after 24h of incubation.

In-situ EPR analysis is an effective method for detecting •OH species [67,68]. In this study, the samples were immersed in an aqueous medium containing DMPO and kept in the dark during the measurements. The EPR spectra, shown in **Figure 6A**, reveal that •OH radicals were trapped by DMPO, with no detectable •OH signals in the absence of the samples. By double integrating the signals between 3380 G and 3460 G, the values (expressed in arbitrary units) corresponding to •OH production were obtained for the SC (9.43), SC1 (38.92), SC2 (18.63), and SC4 (12.98) samples. The intensity of the signals attributed to the DMPO-OH adduct decreased as the amount of WO_3:Ag on the carbon support surface increased, indicating that •OH production is influenced by the synergy between WO_3:Ag and the carbon support. In this context, it can be observed that the SC1 and SC2 samples produce a higher amount of •OH radicals, which may explain their increased efficiency in eliminating MB49 cells.

The generation of •OH radicals and other reactive species such as •OOH, $^1O_2$, h^+ (low electronic density), and e^- (high electronic density) by the samples was investigated by adding specific scavengers for these species during the photodegradation of RhB (**Figure 6B**) [69]. As expected, the SC sample showed minimal RhB photodegradation, indicating limited production of these reactive species by carbon support. In contrast, samples SC1, SC2, and SC4 displayed increased RhB photodegradation, which correlated with WO_3:Ag heterostructure, with SC2 being the most effective. The decrease in RhB photodegradation efficiency by the SC4 sample may be related to the excess WO_3:Ag, which reduces the charge pair separation efficiency provided by the carbon support. The addition of reactive scavengers led to a reduction in photocatalytic efficiency across all tests, with the most pronounced decrease observed for •OH, h^+, and e^-. The decrease in efficiency for •OOH and $^1O_2$ suggests that these species are also being produced during the process, indicating that •OH radical generation is not exclusive. These findings suggest that these reactive species contribute to the biological activity of the samples even in the absence of light, supporting the EPR analysis shown earlier.

The release of Ag^+ and W^{6+} into the solution was investigated using ICP-OES over a 24-hour period (**Figure 6C**). The samples were incubated at various concentrations in the culture medium. It was observed that both Ag^+ and W^{6+} exhibited minimal ionic release, with amounts less than 0.01% (<0.6 ppb). Therefore, the cytotoxic effects are primarily attributed to the production of ROS by the SC1 and SC2 samples. According to previously published studies,

these concentrations of Ag^{+} and W^{6+} ions are not toxic [70–72].

These results, along with the analysis of ROS production, demonstrate that it is indeed possible to control ionic release and ROS generation by using a carbon support, which was one of the main objectives of this work in aiming to facilitate the biological application of these materials. In previous studies, when compared to the direct use of α-Ag_2WO_4, the 24-hour ionic release at comparable concentrations reached 2.36 ppm [70]. Despite the initial α-Ag_2WO_4 content being only 10% of the sample weight, this value is still nearly 500 times lower, highlighting the improved control offered by the carbon support. While ROS production via photocatalysis is more qualitative than quantitative, making direct comparison challenging due to varying concentrations of RhB, photocatalyst, and system specifications, the different amounts of starting reactants, chitosan and α-Ag_2WO_4 used to obtain the WO_3:Ag heterostructures supported on carbon, indicate that ROS production efficiency can be regulated. Therefore, the thermal decomposition process, coupled with the use of a carbon support, is critical in determining the reactive behavior of this material.

To understand the mechanism of action of this material, it is crucial to consider the effects of Ag on the WO_3 semiconductor. When the work function of Ag (Φ_M^{Ag}) is lower than the electron affinity of WO_3 ($\chi_S^{WO_3}$), the semiconductor gains a negative charge, causing a downward shift at the interface [73]. As previously observed, •OH radicals are generated even in the absence of light, indicating that excited electrons in the conduction band (CB) promote electron deficiency (h^{+}) in the valence band (VB), enabling redox reactions [74,75]. This results in electron accumulation at the interface (e^{-}), establishing a contact potential between WO_3 and Ag. The rapid electronic transfer between the CB and VB occurs at the contact interface, leading to efficient charge separation and reinforcing the contact potential between the two materials [76]. Recombination traps in the forbidden energy region (E_{gap}) of WO_3 (2.8 eV) enhance the recombination process (Figure 7A). The formation of these distinct electronic densities is essential for the production of ROS through interactions with H_2O and O_2 molecules (Figure 7B). The electron deficiency interacts with H_2O molecules, forming •OH radicals and protons (H^{+}), while the accumulated electron density reacts with O_2 to generate superoxide radical ($•O_2^{-}$). The $•O_2^{-}$ then combines with H^{+} to form •OOH or loose an e^{-} to form $^1O_2$ **[77]**

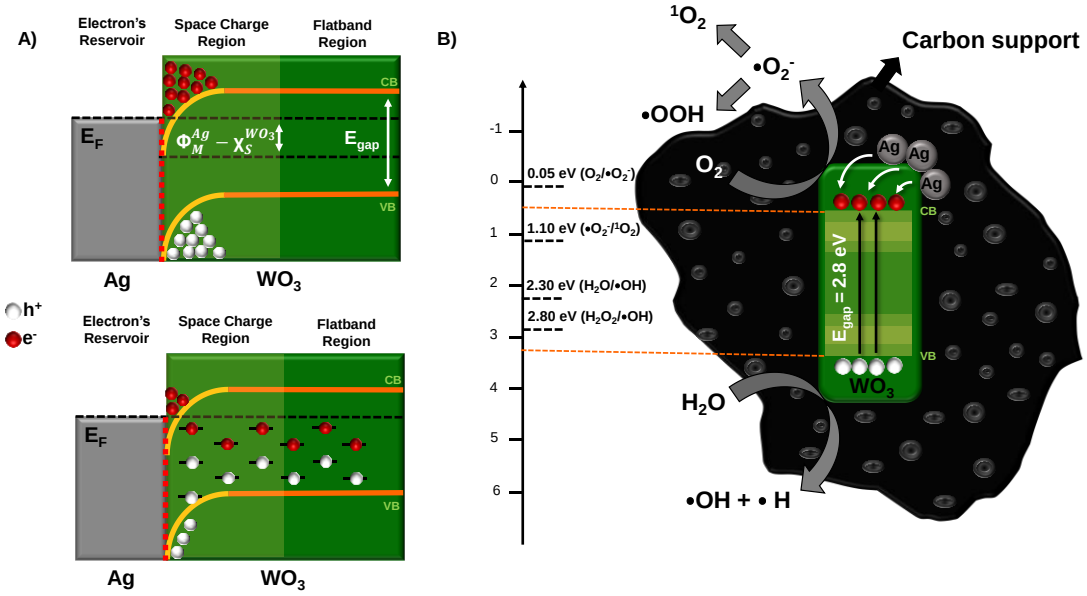

.Figure 7. A) Interface and B) ROS formation schema by WO_3:Ag heterostructures supported on carbon.

These species can penetrate cell membranes and interact with phosphate and sulfate groups, leading to cell death or inhibition of cell replication by disrupting essential protein synthesis and causing damage to DNA [78,79]. Due to the short lifetime of ROS, most of the damage occurs in the cell wall, affecting cellular respiration and altering the electrochemical potential of cells [80].

5. CONCLUSIONS

The study demonstrated that WO_3:Ag heterostructures supported on carbon, synthesized through the thermal decomposition of α-Ag_2WO_4 in a chitosan matrix, exhibited a porous structure with uniformly distributed particles, enabling efficient control of ionic release and the generation of reactive oxygen species (ROS). The SC1 and SC2 samples showed high efficacy in reducing the viability

of bladder carcinoma cells (MB49) with lower toxicity to murine fibroblasts (3T3), indicating apoptosis induced by increased ROS levels and caspase-3 activation, while the low release of Ag^{+} and W^{6+} ions (<0.01%) reinforced the material's safety. The synergistic interaction between WO_3 and Ag, along with the carbon support, was crucial for modulating the generation of •OH and other reactive species, even in the absence of light, highlighting the potential of these heterostructures as a promising strategy for bladder cancer treatment.

ACKNOWLEDGMENTS

This study was funded by the São Paulo Research Foundation (FAPESP) (2013/07296-2 and 2022/06210-6). M.A. was supported by a FAPESP postdoctoral fellowship (2023/08525-7). J.M.A.R. and K.F.G. were supported by a Petrobras postdoctoral fellowship (2022/00220-0). The authors express their gratitude to Dr. Heloisa Sobreiro Selistre de Araújo and Dr. Marisa Narciso (Department of Physiological Sciences, Federal University of São Carlos, São Carlos, SP, Brazil), as well as Dr. Márcia Regina Cominetti (Department of Gerontology, Federal University of São Carlos, São Carlos, SP, Brazil), for providing essential equipment used in some of the analyses.

AUTHOR CONTRIBUTIONS

B.L.D.F. and **J.M.A.R.:** Conceptualization, Methodology, Investigation, Data Curation, Analysis, Validation, Writing - Original Draft, Writing - Review & Editing. **B.L.D.F.**, **J.M.A.R**, **K.F.G**, and **M.A:** Data Curation, Analysis, Writing - Review & Editing. **L.O.L**, **L.I.G** and **M.S.C.**: Data Curation, Analysis. **A.C.M.R.**, **F.F.A.** and **E.L.:** Supervision, Resources, Funding Acquisition, Writing - Review & Editing.

CONFLICT OF INTEREST STATEMENT

The authors declare that they have no conflicting financial interests or personal relationships that could have appeared to influence the work.

REFERENCES

I. B.W. Stewart, C.P. Wild, WORLD CANCER REPORT 2014, 2014.

II. Globocan, International Agency for Research on Cancer. WHO Chron 23 (2020) 323–326.

III. I. et al. JUBBER, Epidemiology of Bladder Cancer in 2023: A Systematic Review of Risk Factors, Eur Urol (2023).

IV. L. Tran, J.F. Xiao, N. Agarwal, J.E. Duex, D. Theodorescu, Advances in bladder cancer biology and therapy, Nat Rev Cancer 21 (2021) 104–121. https://doi.org/10.1038/s41568-020-00313-1.

V. M.S. Lawrence, P. Stojanov, P. Polak, G. V. Kryukov, K. Cibulskis, A. Sivachenko, S.L. Carter, C. Stewart, C.H. Mermel, S.A. Roberts, A. Kiezun, P.S. Hammerman, A. McKenna, Y. Drier, L. Zou, A.H. Ramos, T.J. Pugh, N. Stransky, E. Helman, J. Kim, C. Sougnez, L. Ambrogio, E. Nickerson, E. Shefler, M.L. Cortés, D. Auclair, G. Saksena, D. Voet, M. Noble, D. Dicara, P. Lin, L. Lichtenstein, D.I. Heiman, T. Fennell, M. Imielinski, B. Hernandez, E. Hodis, S. Baca, A.M. Dulak, J. Lohr, D.A. Landau, C.J. Wu, J. Melendez-Zajgla, A. Hidalgo-Miranda, A. Koren, S.A. McCarroll, J. Mora, R.S. Lee, B. Crompton, R. Onofrio, M. Parkin, W. Winckler, K. Ardlie, S.B. Gabriel, C.W.M. Roberts, J.A. Biegel, K. Stegmaier, A.J. Bass, L.A. Garraway, M. Meyerson, T.R. Golub, D.A. Gordenin, S. Sunyaev, E.S. Lander, G. Getz, Mutational heterogeneity in cancer and the search for new cancer-associated genes, Nature 499 (2013) 214–218. https://doi.org/10.1038/nature12213.

VI. L.B. Alexandrov, S. Nik-Zainal, D.C. Wedge, S.A.J.R. Aparicio, S. Behjati, A. V. Biankin, G.R. Bignell, N. Bolli, A. Borg, A.L. Børresen-Dale, S. Boyault, B. Burkhardt, A.P. Butler, C. Caldas, H.R. Davies, C. Desmedt, R. Eils, J.E. Eyfjörd, J.A. Foekens, M. Greaves, F. Hosoda, B. Hutter, T. Ilicic, S. Imbeaud, M. Imielinsk, N. Jäger, D.T.W. Jones, D. Jonas, S. Knappskog, M. Koo, S.R. Lakhani, C. López-Otín, S. Martin, N.C. Munshi, H. Nakamura, P.A. Northcott, M. Pajic, E. Papaemmanuil, A. Paradiso, J. V. Pearson, X.S. Puente, K. Raine, M. Ramakrishna, A.L. Richardson, J. Richter, P. Rosenstiel, M. Schlesner, T.N. Schumacher, P.N. Span, J.W. Teague, Y. Totoki, A.N.J. Tutt, R. Valdés-Mas, M.M. Van Buuren, L. Van 'T Veer, A. Vincent-Salomon, N. Waddell, L.R. Yates, J. Zucman-Rossi, P. Andrew Futreal, U. McDermott, P. Lichter, M. Meyerson, S.M. Grimmond, R. Siebert, E. Campo, T. Shibata, S.M. Pfister, P.J. Campbell, M.R. Stratton, Signatures of mutational processes in human cancer, Nature 500 (2013) 415–421. https://doi.org/10.1038/nature12477.

VII. C.S. Garris, J.L. Wong, J. V. Ravetch, D.A. Knorr, Dendritic cell targeting with Fc-enhanced CD40 antibody agonists induces durable antitumor immunity in humanized mouse models of bladder cancer, Sci Transl Med 13 (2021). https://doi.org/10.1126/scitranslmed.abd1346.

VIII. B.A. John, N. Said, Insights from animal models of bladder cancer: recent advances, challenges, and opportunities, Oncotarget 8 (2017) 57766–57781. https://doi.org/10.18632/oncotarget.17714.

IX. Y. Zhu, S. Pang, C. Lei, Y. Luo, Q. Chu, W. Tan, Development of a therapy against metastatic bladder cancer using an interleukin-2 surface-modified

MB49 bladder cancer stem cells vaccine, Stem Cell Res Ther 6 (2015) 224. https://doi.org/10.1186/s13287-015-0211-1.

X. M. Burger, J.W.F. Catto, G. Dalbagni, H.B. Grossman, H. Herr, P. Karakiewicz, W. Kassouf, L.A. Kiemeney, C. La Vecchia, S. Shariat, Y. Lotan, Epidemiology and risk factors of urothelial bladder cancer, Eur Urol 63 (2013) 234–241. https://doi.org/10.1016/j.eururo.2012.07.033.

XI. A. Jurj, C. Braicu, L.A. Pop, C. Tomuleasa, C.D. Gherman, I. Berindan-Neagoe, The new era of nanotechnology, an alternative to change cancer treatment, Drug Des Devel Ther 11 (2017) 2871–2890. https://doi.org/10.2147/DDDT.S142337.

XII. And Bawendi.M.G. Murray, C. B., Kagan.R., Synthesis and Characterization of Monodisperse Nanocrystals and Close-Packed Nanocrystal Assemblies, Annual Review of Materials Science 30 (2006) 545–610.

XIII. A.R.C. Braga, L.G. Trindade, S.P. Ramos, M. Bürck, M.M. Nakamoto, L.R. Bernardo, L.O. Libero, A.F. Gouveia, M. Assis, Design Ag-Based Semiconductors for Antimicrobial Technologies: Challenges and Future Trends, in: Nanomaterials for Biomedical and Bioengineering Applications, Springer Nature Singapore, Singapore, 2024: pp. 277–300. https://doi.org/10.1007/978-981-97-0221-3_11.

XIV. A. Azam, A.S. Ahmed, M. Oves, M.S. Khan, S.S. Habib, A. Memic, Antimicrobial activity of metal oxide nanoparticles against Gram-positive and Gram-negative bacteria: A comparative study, Int J Nanomedicine 7 (2012) 6003–6009. https://doi.org/10.2147/IJN.S35347.

XV. H. Qin, H. Cao, Y. Zhao, C. Zhu, T. Cheng, Q. Wang, X. Peng, M. Cheng, J. Wang, G. Jin, Y. Jiang, X. Zhang, X. Liu, P.K. Chu, In vitro and in vivo anti-biofilm effects of silver nanoparticles immobilized on titanium, Biomaterials 35 (2014) 9114–9125. https://doi.org/10.1016/j.biomaterials.2014.07.040.

XVI. T. Bruna, F. Maldonado-Bravo, P. Jara, N. Caro, Silver nanoparticles and their antibacterial applications, Int J Mol Sci 22 (2021). https://doi.org/10.3390/ijms22137202.

XVII. D. Bamal, A. Singh, G. Chaudhary, M. Kumar, M. Singh, N. Rani, P. Mundlia, A.R. Sehrawat, Silver nanoparticles biosynthesis, characterization, antimicrobial activities, applications, cytotoxicity and safety issues: An updated review, Nanomaterials 11 (2021). https://doi.org/10.3390/nano11082086.

XVIII. Z.A. Ratan, M.F. Haidere, Md. Nurunnabi, S.Md. Shahriar, A.J.S. Ahammad, Y.Y. Shim, M.J.T. Reaney, J.Y. Cho, Green Chemistry Synthesis of Silver Nanoparticles and Their Potential Anticancer Effects, Cancers (Basel) 12 (2020) 855. https://doi.org/10.3390/cancers12040855.

XIX. K. Y, N. M, A. M, K. AT, A. T, A. N, S. ZK, Bio-Synthesized Silver Nanoparticles Using Different Plant Extracts as Anti-Cancer Agent, J Nanomedine Biotherapeutic Discov 07 (2017). https://doi.org/10.4172/2155-983X.1000154.

XX. Y. Hiraku, Y. Nishikawa, N. Ma, T. Afroz, K. Mizobuchi, R. Ishiyama, Y. Matsunaga, T. Ichinose, S. Kawanishi, M. Murata, Nitrative DNA damage induced by carbon-black nanoparticles in macrophages and lung epithelial cells, Mutat Res Gen Tox En 818 (2017) 7–16. https://doi.org/10.1016/j.mrgentox.2017.04.002.

XXI. A.F. Gouveia, R.A. Roca, N.G. Macedo, L.S. Cavalcante, E. Longo, M.A. San-Miguel, A. Altomare, G.S. da Silva, J. Andrés, Ag2WO4 as a multifunctional material: Fundamentals and progress of an extraordinarily versatile semiconductor, Journal of Materials Research and Technology 21 (2022) 4023–4051. https://doi.org/10.1016/j.jmrt.2022.11.011.

XXII. M. Assis, E. Cordoncillo, R. Torres-Mendieta, H. Beltrán-Mir, G. Mínguez-Vega, R. Oliveira, E.R. Leite, C.C. Foggi, C.E. Vergani, E. Longo, J. Andrés, Towards the scale-up of the formation of nanoparticles on α-Ag2WO4 with bactericidal properties by femtosecond laser irradiation, Sci Rep 8 (2018) 1884. https://doi.org/10.1038/s41598-018-19270-9.

XXIII. N.G. Macedo, T.R. Machado, R.A. Roca, M. Assis, C.C. Foggi, V. Puerto-Belda, G. Mínguez-Vega, A. Rodrigues, M.A. San-Miguel, E. Cordoncillo, H. Beltrán-Mir, J. Andrés, E. Longo, Tailoring the Bactericidal Activity of Ag Nanoparticles/α-Ag 2 WO 4 Composite Induced by Electron Beam and Femtosecond Laser Irradiation: Integration of Experiment and Computational Modeling, ACS Appl Bio Mater 2 (2019) 824–837. https://doi.org/10.1021/acsabm.8b00673.

XXIV. B.N.A. da S. Pimentel, F.H. Marin-Dett, M. Assis, P.A. Barbugli, E. Longo, C.E. Vergani, Antifungal Activity and Biocompatibility of α-AgVO3, α-Ag2WO4, and β-Ag2MoO4 Using a Three-Dimensional Coculture Model of the Oral Mucosa, Front Bioeng Biotechnol 10 (2022). https://doi.org/10.3389/fbioe.2022.826123.

XXV. L.O. Laier, M. Assis, C.C. Foggi, A.F. Gouveia, C.E. Vergani, L.C.L. Santana, L.S. Cavalcante, J. Andrés, E. Longo, Surface-dependent properties of α-Ag2WO4: a joint experimental and theoretical investigation, Theor Chem Acc 139 (2020) 108. https://doi.org/10.1007/s00214-020-02613-z.

XXVI. M. Assis, L.K. Ribeiro, M.O. Gonçalves, L.H. Staffa, R.S. Paiva, L.R. Lima, D. Coelho, L.F. Almeida, L.N. Moraes, I.L. V. Rosa, L.H. Mascaro, R.M.T. Grotto, C.P. Sousa, J. Andrés, E. Longo, S.A. Cruz, Polypropylene Modified with Ag-Based Semiconductors as a Potential Material against SARS-CoV-2 and Other Pathogens, ACS Appl Polym Mater 4 (2022) 7102–7114. https://doi.org/10.1021/acsapm.2c00744.

XXVII. L.A. Onue, L.K. Ribeiro, M.O. Gonçalves, E. Longo, C. Paiva de Sousa, M. Assis, S.A. Cruz, Unveiling Antimicrobial Properties and Crystallization Induction in PLA Using α-Ag 2 WO 4 Nanoparticles, ACS Appl Polym Mater 6 (2024) 3233–3242. https://doi.org/10.1021/acsapm.3c03012.

XXVIII. M. Assis, A.F. Gouveia, L.K. Ribeiro, M.A. Ponce, M.S. Churio, O.N. Oliveira, L.H. Mascaro, E. Longo, R. Llusar, E. Guillamón, J. Andrés, Towards an efficient selective oxidation of sulfides to sulfones by NiWO and α-AgWO, Appl Catal A Gen 652 (2023) 119038. https://doi.org/10.1016/j.apcata.2023.119038.

XXIX. L.K. Ribeiro, A.F. Gouveia, F. das C.M. Silva, L.F.G. Noleto, M. Assis, A.M. Batista, L.S. Cavalcante, E. Guillamón, I.L. V. Rosa, E. Longo, J. Andrés, G.E. Luz Júnior, Tug-of-War Driven by the Structure of Carboxylic Acids: Tuning the Size, Morphology, and Photocatalytic Activity of α-Ag2WO4, Nanomaterials 12 (2022) 3316. https://doi.org/10.3390/nano12193316.

XXX. B.D.L. Fragelli, M. Assis, J.M.A. Rodolpho, K.F. Godoy, L.O. Líbero, F.F. Anibal, E. Longo, Modulation of cell death mechanisms via α-Ag2WO4 morphology-dependent factors, J Photochem Photobiol B 257 (2024) 112947. https://doi.org/10.1016/j.jphotobiol.2024.112947.

XXXI. C.B. de Abreu, R.C. Gebara, L.L. dos Reis, G.S. Rocha, L.O.G. Alho, L.M. Alvarenga, L.S. Virtuoso, M. Assis, A. da S. Mansano, E. Longo, M. da G.G. Melão, Effects of α-Ag2WO4 crystals on photosynthetic efficiency and biomolecule composition of the algae Raphidocelis subcapitata, Water Air Soil Pollut 233 (2022) 121. https://doi.org/10.1007/s11270-022-05604-x.

XXXII. C.B. de Abreu, R.C. Gebara, L.L. dos Reis, G.S. Rocha, L. de O.G. Alho, L.M. Alvarenga, L.S. Virtuoso, M. Assis, A. da S. Mansano, E. Longo, M. da G.G. Melão, Toxicity of α-Ag2WO4 microcrystals to freshwater microalga Raphidocelis subcapitata at cellular and population levels, Chemosphere 288 (2022) 132536. https://doi.org/10.1016/j.chemosphere.2021.132536.

XXXIII. M. Assis, T. Robeldo, C.C. Foggi, A.M. Kubo, G. Mínguez-Vega, E. Condoncillo, H. Beltran-Mir, R. Torres-Mendieta, J. Andrés, M. Oliva, C.E. Vergani, P.A. Barbugli, E.R. Camargo, R.C. Borra, E. Longo, Ag Nanoparticles/α-Ag2WO4 Composite Formed by Electron Beam and Femtosecond Irradiation as Potent Antifungal and Antitumor Agents, Sci Rep 9 (2019) 9927. https://doi.org/10.1038/s41598-019-46159-y.

XXXIV. Y. Cai, Y. Liu, W. Yan, Q. Hu, J. Tao, M. Zhang, Z. Shi, R. Tang, Role of hydroxyapatite nanoparticle size in bone cell proliferation, J Mater Chem 17 (2007) 3780–3787. https://doi.org/10.1039/b705129h.

XXXV. S. Metwally, U. Stachewicz, Surface potential and charges impact on cell responses on biomaterials interfaces for medical applications, Materials Science and Engineering C 104 (2019) 109883. https://doi.org/10.1016/j.msec.2019.109883.

XXXVI. L.E. Feinendegen, Reactive oxygen species in cell responses to toxic agents, Hum Exp Toxicol 21 (2002) 85–90. https://doi.org/10.1191/0960327102ht216oa.

XXXVII. P.P. Fu, Q. Xia, H.M. Hwang, P.C. Ray, H. Yu, Mechanisms of nanotoxicity: Generation of reactive oxygen species, J Food Drug Anal 22 (2014) 64–75. https://doi.org/10.1016/j.jfda.2014.01.005.

XXXVIII. L.Z. Flores-López, H. Espinoza-Gómez, R. Somanathan, Silver nanoparticles: Electron transfer, reactive oxygen species, oxidative stress, beneficial and toxicological effects. Mini review, Journal of Applied Toxicology 39 (2019) 16–26. https://doi.org/10.1002/jat.3654.

XXXIX. M. Assis, M.S. Castro, C.M. Aldao, C. Buono, P.P. Ortega, M.D. Teodoro, J. Andrés, A.F. Gouveia, A.Z. Simões, E. Longo, C.E. Macchi, A. Somoza, F. Moura, M.A. Ponce, Disclosing the nature of vacancy defects in α-Ag2WO4, Mater Res Bull 164 (2023) 112252. https://doi.org/10.1016/j.materresbull.2023.112252.

XL. K.L. Patrocinio, J.R. Santos, L.I. Granone, M.A. Ponce, M.S. Churio, L.K. Ribeiro, M.D. Teodoro, R. Llusar, J. Andrés, E. Longo, M. Assis, Tuning the morphology to enhance the catalytic activity of α-Ag 2 WO 4 through V-doping, Dalton Transactions 52 (2023) 14982–14994. https://doi.org/10.1039/D3DT02352D.

XLI. ATCC - American Type Culture Collection, NIH/3T3, (n.d.).

XLII. F. Chen, G. Zhang, Y. Cao, M.J. Hessner, W.A. See, MB49 Murine Urothelial Carcinoma: Molecular and Phenotypic Comparison to Human Cell Lines as a Model of the Direct Tumor Response to Bacillus Calmette-Guerin, Journal of Urology 182 (2009)

2932–2937. https://doi.org/10.1016/j.juro.2009.08.018.

XLIII. Tim. Mosmann, Rapid Colorimetric Assay for Cellular Growth and Survival: Application to Proliferation and Cytotoxicity Assays, J Immunol Methods 65 (1983) 55–63. https://doi.org/10.1039/c6ra17788c.

XLIV. G. Repetto, A. del Peso, J.L. Zurita, Neutral red uptake assay for the estimation of cell viability/ cytotoxicity, Nat Protoc 3 (2008) 1125–1131. https://doi.org/10.1038/nprot.2008.75.

XLV. W.K. Martins, D. Severino, C. Souza, B.S. Stolf, M.S. Baptista, Rapid screening of potential autophagic inductor agents using mammalian cell lines, Biotechnol J 8 (2013) 730–737. https://doi.org/10.1002/biot.201200306.

XLVI. L.C. Green, D.A. Wagner, J. Glogowski, P.L. Skipper, J.S. Wishnok, S.R. Tannenbaum, Analysis of nitrate, nitrite, and [15N]nitrate in biological fluids, Anal Biochem 126 (1982) 131–138. https://doi.org/10.1016/0003-2697(82)90118-X.

XLVII. L.A. Ramos, C.C.S. Cavalheiro, É.T.G. Cavalheiro, Determinação de nitrito em águas utilizando extrato de flores, Quim Nova 29 (2006) 1114–1120. https://doi.org/10.1590/S0100-40422006000500037.

XLVIII. B.E. Saltzman, Colorimetric Microdetermination of Nitrogen Dioxide in the Atmosphere, Anal Chem 26 (1954) 1949–1955. https://doi.org/10.1021/ac60096a025.

XLIX. D. Mustika, T. Torowati, S. Sudirman, A. Fisli, I.M. Joni, R. Langenati, J. Setiawan, Purification of Indonesian Natural Graphite by Acid Leaching Method as Nuclear Fuel Matrix: Physical Characterization, Int J Chem 11 (2019) 9. https://doi.org/10.5539/ijc.v11n1p9.

L. E.Z. da Silva, G.M. Faccin, T.R. Machado, N.G. Macedo, M. de Assis, S. Maya-Johnson, J.C. Sczancoski, J. Andrés, E. Longo, M.A. San-Miguel, Connecting Theory with Experiment to Understand the Sintering Processes of Ag Nanoparticles, The Journal of Physical Chemistry C 123 (2019) 11310–11318. https://doi.org/10.1021/acs.jpcc.9b02107.

LI. H. Simchi, B.E. McCandless, T. Meng, W.N. Shafarman, Structural, optical, and surface properties of WO3 thin films for solar cells, J Alloys Compd 617 (2014) 609–615. https://doi.org/10.1016/j.jallcom.2014.08.047.

LII. B. Salesa, A. Tuñón-Molina, A. Cano-Vicent, M. Assis, J. Andrés, Á. Serrano-Aroca, Graphene Nanoplatelets: In Vivo and In Vitro Toxicity, Cell Proliferative Activity, and Cell Gene Expression, Applied Sciences 12 (2022) 720. https://doi.org/10.3390/app12020720.

LIII. K. Zhang, X. Zhang, H. Li, X. Xing, L. Jin, Q. Cao, P. Li, Direct exfoliation of graphite into graphene in aqueous solution using a novel surfactant obtained from used engine oil, J Mater Sci 53 (2018) 2484–2496. https://doi.org/10.1007/s10853-017-1729-7.

LIV. L. Zhou, H.J. Forman, Y. Ge, J. Lunec, Multi-walled carbon nanotubes: A cytotoxicity study in relation to functionalization, dose and dispersion, Toxicology in Vitro 42 (2017) 292–298. https://doi.org/10.1016/j.tiv.2017.04.027.

LV. B.D.L. Fragelli, M. Assis, J.M.A. Rodolpho, K.F. Godoy, L.O. Líbero, F.F. Anibal, E. Longo, Modulation of cell death mechanisms via α-Ag2WO4 morphology-dependent factors, J Photochem Photobiol B 257 (2024). https://doi.org/10.1016/j.jphotobiol.2024.112947.

LVI. A.B. Apolo, N.J. Vogelzang, D. Theodorescu, New and Promising Strategies in the Management of Bladder Cancer, 2015. https://doi.org/10.14694/EdBook_AM.2015.35.105

LVII. G. Annamalai, S. Kathiresan, N. Kannappan, [6]-Shogaol, a dietary phenolic compound, induces oxidative stress mediated mitochondrial dependant apoptosis through activation of proapoptotic factors in Hep-2 cells, Biomedicine & Pharmacotherapy 82 (2016) 226–236. https://doi.org/10.1016/j.biopha.2016.04.044.

LVIII. D.B. Zorov, M. Juhaszova, S.J. Sollott, Mitochondrial ROS-induced ROS release: An update and review, Biochimica et Biophysica Acta (BBA) - Bioenergetics 1757 (2006) 509–517. https://doi.org/10.1016/j.bbabio.2006.04.029.

LIX. Q. Xie, Z. Yuan, H. Hou, H. Zhao, H. Chen, X. Ni, Effects of ROS and caspase-3-like protein on the growth and aerenchyma formation of Potamogeton perfoliatus stem, Protoplasma 260 (2023) 307–325. https://doi.org/10.1007/s00709-022-01780-z.

LX. D.B. Zorov, C.R. Filburn, L.-O. Klotz, J.L. Zweier, S.J. Sollott, Reactive Oxygen Species (Ros-Induced) Ros Release, J Exp Med 192 (2000) 1001–1014. https://doi.org/10.1084/jem.192.7.1001.

LXI. A.S. Fomicheva, A.I. Tuzhikov, R.E. Beloshistov, S. V. Trusova, R.A. Galiullina, L. V. Mochalova, N. V. Chichkova, A.B. Vartapetian, Programmed cell death in plants, Biochemistry (Moscow) 77 (2012) 1452–1464. https://doi.org/10.1134/S0006297912130044.

LXII. E. Eskandari, C.J. Eaves, Paradoxical roles of caspase-3 in regulating cell survival, proliferation, and tumorigenesis, Journal of Cell Biology 221 (2022). https://doi.org/10.1083/jcb.202201159.

LXIII. E. Eskandari, C.J. Eaves, Paradoxical roles of caspase-3 in regulating cell survival, proliferation,

and tumorigenesis, Journal of Cell Biology 221 (2022). https://doi.org/10.1083/jcb.202201159.

LXIV. A.A. Bhat, R. Thapa, O. Afzal, N. Agrawal, W.H. Almalki, I. Kazmi, S.I. Alzarea, A.S.A. Altamimi, P. Prasher, S.K. Singh, K. Dua, G. Gupta, The pyroptotic role of Caspase-3/GSDME signalling pathway among various cancer: A Review, Int J Biol Macromol 242 (2023) 124832. https://doi.org/10.1016/j.ijbiomac.2023.124832.

LXV. M. Godoy-Gallardo, U. Eckhard, L.M. Delgado, Y.J.D. de Roo Puente, M. Hoyos-Nogués, F.J. Gil, R.A. Perez, Antibacterial approaches in tissue engineering using metal ions and nanoparticles: From mechanisms to applications, Bioact Mater 6 (2021) 4470–4490. https://doi.org/10.1016/j.bioactmat.2021.04.033.

LXVI. L. Wang, C. Hu, L. Shao, The antimicrobial activity of nanoparticles: present situation and prospects for the future, Int J Nanomedicine Volume 12 (2017) 1227–1249. https://doi.org/10.2147/IJN.S121956.

LXVII. L.O. Libero, L.K. Ribeiro, L.I. Granone, M.S. Churio, J.C. Souza, V.R. Mastelaro, J. Andrés, E. Longo, L.H. Mascaro, M. Assis, Introducing Structural Diversity: Fe 2 (MoO 4) 3 Immobilized in Chitosan Films as an Efficient Catalyst for the Selective Oxidation of Sulfides to Sulfones, ChemCatChem 15 (2023). https://doi.org/10.1002/cctc.202300421.

LXVIII. S.K. Han, T.-M. Hwang, Y. Yoon, J.-W. Kang, Evidence of singlet oxygen and hydroxyl radical formation in aqueous goethite suspension using spin-trapping electron paramagnetic resonance (EPR), Chemosphere 84 (2011) 1095–1101. https://doi.org/10.1016/j.chemosphere.2011.04.051.

LXIX. M. Assis, T. Robeldo, C.C. Foggi, A.M. Kubo, G. Mínguez-Vega, E. Condoncillo, H. Beltran-Mir, R. Torres-Mendieta, J. Andrés, M. Oliva, C.E. Vergani, P.A. Barbugli, E.R. Camargo, R.C. Borra, E. Longo, Ag Nanoparticles/α-Ag2WO4 Composite Formed by Electron Beam and Femtosecond Irradiation as Potent Antifungal and Antitumor Agents, Sci Rep 9 (2019) 9927. https://doi.org/10.1038/s41598-019-46159-y.

LXX. S. Chinde, N. Dumala, M.F. Rahman, S.S.K. Kamal, S.I. Kumari, M. Mahboob, P. Grover, Toxicological assessment of tungsten oxide nanoparticles in rats after acute oral exposure, Environmental Science and Pollution Research 24 (2017) 13576–13593. https://doi.org/10.1007/s11356-017-8892-x.

LXXI. E. Caballero-Díaz, C. Pfeiffer, L. Kastl, P. Rivera-Gil, B. Simonet, M. Valcárcel, J. Jiménez-Lamana, F. Laborda, W.J. Parak, The Toxicity of Silver Nanoparticles Depends on Their Uptake by Cells and Thus on Their Surface Chemistry, Particle & Particle Systems Characterization 30 (2013) 1079–1085. https://doi.org/10.1002/ppsc.201300215.

LXXII. F. Sambale, S. Wagner, F. Stahl, R.R. Khaydarov, T. Scheper, D. Bahnemann, Investigations of the Toxic Effect of Silver Nanoparticles on Mammalian Cell Lines, J Nanomater 2015 (2015). https://doi.org/10.1155/2015/136765.

LXXIII. R.A. Capeli, T. Belmonte, J. Caierão, C.J. Dalmaschio, S.R. Teixeira, V.R. Mastelaro, A.J. Chiquito, M.D. Teodoro, J.F.M. Domenegueti, E. Longo, L.G. Trindade, F.M. Pontes, Effect of hydrothermal temperature on the antibacterial and photocatalytic activity of WO3 decorated with silver nanoparticles, J Solgel Sci Technol 97 (2021) 228–244. https://doi.org/10.1007/s10971-020-05433-6.

LXXIV. M. Assis, M.S. Castro, C.M. Aldao, C. Buono, P.P. Ortega, M.D. Teodoro, J. Andrés, A.F. Gouveia, A.Z. Simões, E. Longo, C.E. Macchi, A. Somoza, F. Moura, M.A. Ponce, Disclosing the nature of vacancy defects in α-Ag2WO4, Mater Res Bull 164 (2023) 112252. https://doi.org/10.1016/j.materresbull.2023.112252.

LXXV. M. Assis, L.G.P. Simoes, G.C. Tremiliosi, L.K. Ribeiro, D. Coelho, D.T. Minozzi, R.I. Santos, D.C.B. Vilela, L.H. Mascaro, J. Andrés, E. Longo, PVC-SiO2-Ag composite as a powerful biocide and anti-SARS-CoV-2 material, Journal of Polymer Research 28 (2021) 361. https://doi.org/10.1007/s10965-021-02729-1.

LXXVI. R. Georgekutty, M.K. Seery, S.C. Pillai, A Highly Efficient Ag-ZnO Photocatalyst: Synthesis, Properties, and Mechanism, The Journal of Physical Chemistry C 112 (2008) 13563–13570. https://doi.org/10.1021/jp802729a.

LXXVII. L.K. Ribeiro, M. Assis, L.R. Lima, D. Coelho, M.O. Gonçalves, R.S. Paiva, L.N. Moraes, L.F. Almeida, F. Lipsky, M.A. San-Miguel, L.H. Mascaro, R.M.T. Grotto, C.P. Sousa, I.L. V. Rosa, S.A. Cruz, J. Andrés, E. Longo, Bioactive Ag 3 PO 4 /Polypropylene Composites for Inactivation of SARS-CoV-2 and Other Important Public Health Pathogens, J Phys Chem B 125 (2021) 10866–10875. https://doi.org/10.1021/acs.jpcb.1c05225.

LXXVIII. M. Assis, J.S. da Silva, M.O. Gonçalves, J.M. de Almeida Rodolpho, B.D. de Lima Fragelli, A.B.P. Corte, L.K. Ribeiro, M.D. Teodoro, F. de Freitas Anibal, C.P. de Sousa, O.N. Oliveira, J. Andrés, E. Longo, Bactericidal activity of Ag4V2O7/β-AgVO3 heterostructures against antibiotic-resistant Klebsiella pneumoniae, Biomaterials Advances 141 (2022) 213097. https://doi.org/10.1016/j.bioadv.2022.213097.

LXXIX. M. Assis, L.K. Ribeiro, M.O. Gonçalves, L.H. Staffa, R.S. Paiva, L.R. Lima, D. Coelho, L.F.

Almeida, L.N. Moraes, I.L. V. Rosa, L.H. Mascaro, R.M.T. Grotto, C.P. Sousa, J. Andrés, E. Longo, S.A. Cruz, Polypropylene Modified with Ag-Based Semiconductors as a Potential Material against SARS-CoV-2 and Other Pathogens, ACS Appl Polym Mater 4 (2022) 7102–7114. https://doi.org/10.1021/acsapm.2c00744.

LXXX. M. Assis, J.S. da Silva, M.O. Gonçalves, J.M. de Almeida Rodolpho, B.D. de Lima Fragelli, A.B.P. Corte, L.K. Ribeiro, M.D. Teodoro, F. de Freitas Anibal, C.P. de Sousa, O.N. Oliveira, J. Andrés, E. Longo, Bactericidal activity of Ag4V2O7/β-AgVO3 heterostructures against antibiotic-resistant Klebsiella pneumoniae, Biomaterials Advances 141 (2022) 213097. https://doi.org/10.1016/j.bioadv.2022.213097.